Insect Biochemistry and Molecular Biology 109 (2019) 63–71

Contents lists available at ScienceDirect

Insect Biochemistry and Molecular Biology

journal homepage: www.elsevier.com/locate/ibmb

Insect hemolymph coagulation: Kinetics of classically and non-classically secreted clotting factors

Martin R. Schmid[1], Alexis Dziedziech[1], Badrul Arefin[1], Thomas Kienzle, Zhi Wang, Munira Akhter, Jakub Berka, Ulrich Theopold[*]

Stockholm University, Department of Molecular Biosciences, The Wenner-Gren Institute, SE-106 91, Stockholm, Sweden

ARTICLE INFO

Keywords:
Drosophila melanogaster
Wounding
Clotting
Secretion
Non-classical secretion
Transglutaminase
Glutactin
Prophenoloxidase
Bacteria
Defense
Septic injury
Hemolymph
Coagulation

ABSTRACT

In most insects, hemolymph coagulation, which is analogous to mammalian blood clotting, involves close collaboration between humoral and cellular components. To gain insights into the secretion of cellular clotting factors, we created tagged versions of three different clotting factors. Our focus was on factors which are released in a non-classical manner and to characterize them in comparison to a protein that is classically released, namely Glutactin (Glt). Transglutaminase-A (Tg) and Prophenoloxidase 2 (PPO2), both of which lack signal peptide sequences, have been previously demonstrated to be released from plasmatocytes and crystal cells (CCs) respectively, the two hemocyte classes in naïve larvae. We found that at the molecular level, Tg secretion resembles the release of tissue transglutaminase in mammals. Specifically, *Drosophila* Tg is associated with vesicular membranes and remains membrane-bound after release, in contrast to Glt, which we found localizes to a different class of vesicles and is integrated into clot fibers. PPO2 on the other hand, is set free from CCs through cytolysis. We confirm that PPO2 is a central component of the cytosolic crystals and find that the distribution of PPO2 appears to vary across crystals and cells. We propose a tentative scheme for the secretory events during early and late hemolymph coagulation.

1. Introduction

Similar to mammalian immunity, insect innate immune reactions often involve both humoral and cellular components (Elrod-Erickson et al., 2000). This applies to the coagulation of insect hemolymph, which serves to both stop bleeding and prevent entry of microbes into tissues and the hemocoel (Theopold et al., 2014). Protein profiling and bioinformatics in *Drosophila melanogaster* have identified structural clot components such as Fondue (Lindgren et al., 2008; Scherfer et al., 2006), the mucin I71-7 (Korayem et al., 2004), hemolectin (Lesch et al., 2007), as well as enzymes that serve to crosslink clot components (Theopold et al., 2002, 2004; Wang et al., 2010). These enzymes include multifunctional *Drosophila* transglutaminase, which in flies exists in two isoforms - one secreted (Tg-A) and one cytosolic (Tg-B) (Shibata et al., 2017). During coagulation, Tg-A has an equivalent function to the coagulation factor XIIIa in human blood which by creating ε-(γ-glutamyl)lysine bonds, it hardens the clot matrix (Shibata and Kawabata, 2018; Wang et al., 2010).

Further consolidation of insect clots is achieved through activation of prophenoloxidase (PPO). PPO is proteolytically activated downstream of bacterial elicitors or during clotting by damage associated molecular patterns (Krautz et al., 2014), most likely independent of microbes (Bidla et al., 2009; Krautz et al., 2014). Two *Drosophila* PPOs (PPO1 and 2) are produced and contained in a specialized cell-type called crystal cells (CCs) while PPO3 is synthesized in lamellocytes. These large flat cells are low in number in naïve larvae but can increase in frequency by *de novo* differentiation or through transdifferentiation from plasmatocytes in reaction to wounds and parasitoid wasp attacks, and they may in part functionally replace plasmatocytes (Anderl et al., 2016; Arefin et al., 2015; Crozatier and Vincent, 2011; Dudzic et al., 2015; Honti et al., 2014; Markus et al., 2005). PPO2 is stored in a crystalline form in membrane-less intracellular inclusions in CCs (Rizki

Abbreviations: Tg, Transglutaminase; Tg-A, Transglutaminase-A; Tg-B, Transglutaminase-B; PPO2, prophenoloxidase II; CCs, Crystal cells; Glt, Glutactin; tTG, tissue Transglutaminase

[*] Corresponding author. Department of Molecular Biosciences, The Wenner-Gren Institute, Svante Arrhenius väg 20c, SE-10691, Stockholm, Sweden.
E-mail addresses: martin.schmid@su.se (M.R. Schmid), alexis.dziedziech@su.se (A. Dziedziech), badrul.arefin@liu.se (B. Arefin), thomas-k1@gmx.net (T. Kienzle), zhiwang33@gmail.com (Z. Wang), munira.akhter@su.se (M. Akhter), berkajakub@seznam.cz (J. Berka), uli.theopold@su.se (U. Theopold).
[1] These authors contributed equally.

https://doi.org/10.1016/j.ibmb.2019.04.007
Received 29 November 2018; Received in revised form 27 March 2019; Accepted 2 April 2019
Available online 08 April 2019

et al., 1980), for which the cells bear their name. Though secreted from different hemocyte classes, both Tg-A and PPOs lack a classical signal peptide which shows that they are exported in an unconventional manner: Tg-A via the release of exosomes (Shibata et al., 2017) and PPOs via cell rupture (Bidla et al., 2007).

Several other clot components appear to be released via classical secretion including Fondue, Hemolectin and Glutactin (Glt). Glt was originally identified as a secretory component of the basement membrane (Olson et al., 1990) and more recently found to be highly enriched in hemocytes and – similar to Fondue – protects against nematode infections (Arefin et al., 2014), though has not yet been formally shown to localize to the clot matrix.

The clot may serve more functions than previously understood. Not only has the clot been determined to be an important effector mechanism against invading pathogens and rapid regeneration of the bridged cuticle, but has also been demonstrated to have specific properties for infectious response against nematodes (Arefin et al., 2014). Thus, understanding and further unveiling the kinetics of clotting has further impact beyond closing the breach of separation between one's self and non-self. In addition, our understanding of how cellular immunity is augmented through non-classical secretion in comparison to classically secreted proteins like Glt, remains limited. Furthermore, clotting components may have additional immunological or physiological functions which could contribute to an organism's overall health and development.

In an effort to illuminate the kinetics of the clotting reaction, we constructed GFP-coupled UAS constructs which were used to observe the spatiotemporal distribution of Tg, PPO2 and Glt within the clot. We were able to demonstrate that Tg and Glt localize within the clot fibers during early clot formation and then PPO2, in late clot formation.

2. Materials and methods

2.1. Drosophila stocks and genetics

The mutant fly stock *PPO1^{Bc}/CyO* (BL1362) was obtained from the Bloomington (BL) stock center (Bloomington, IN). The *w^{1118iso}* fly strain, obtained from the Szeged *Drosophila* stock center (Szeged, Hungary), was used as a wildtype control (Schmid et al., 2016). The *GAL4/UAS* system was used to drive tissue-specific gene expression of transgenes under *UAS*-control (Brand and Perrimon, 1993). For ubiquitous expression, we used *y^{1}w*; P{w[+mC] = Act5C-GAL4}17bFO1/TM6B, Tb^{1}*, (BL6675). Specific expression in all normally occurring hemocytes or in crystal cells alone was achieved with *w^{1118}; P{Hml-GAL4.Δ}2* (BL30139) or *P{GawB}lzgal4; P{UAS-GFP.S65T}Myo31DFT2* (BL6313) GAL4 driver lines, respectively. From the latter, the *UAS-GFP* was crossed out for experiments in which other constructs under *UAS*-control were to be expressed. These included: *y^{+} Ser^{1}* (BL19120), *y[1] w[*]; P{w[+mC] = UAS-mCD8.mRFP.LG}18a* (BL27398) as well as *y^{1} w*; P{UAS-mCD8::GFP.L}LL5* (108068) from the Kyoto collection. The fusion construct, *w; UAS-mCherry:myc:2xFYVE[2]* was a gift from Amy Kiger (UC San Diego) and has been described previously (Jean et al., 2012). The hemocyte reporter line, *eater-DsRed* was obtained from the lab of Robert Schulz and has been described to be plasmatocyte specific (Tokusumi et al., 2009). Where possible, first chromosomes were exchanged to *w^{1118iso}* from the wt control line.

2.2. Drosophila lines created for this study

Expression constructs were created using Gateway cloning technology. Fully sequenced cDNA clones were used to generate full-length fusion proteins. We used the pTWG vector with a UAS promoter, and EGFP tag at the C—terminus. Primers used for cloning were:

TG-fw: CACCATGGGTCAAAAACTATCGTGTTGCC;
TG-rv: AGCTATTACATCGGTGCGCCTG;
PPO2-fw: CACCATGGCCGACAAGAAGAATCTCCTCC;
PPO2-rv: GTTTGGGCGCTGCACGGTGC:
Glt-fw: CACCATGAAGCCGTTGCTCCTAGTGTTGG;
Glt-rv: GTTCCGAGAATTGCGTTCCCTCTCT.

All constructs were verified by sequencing. UAS-Tg::GFP, UAS-Glt::GFP, and UAS-PPO2::GFP were injected into fly embryos and transgenic *Drosophila* lines mapped and balanced. Expression strength was validated through Western blotting using GFP-specific antibodies as shown in Fig. S1 and based on strength of fluoresence of GFP, three lines were chosen for each construct including strong, medium and weak expression (two GAL4 lines for each).

2.3. Fly crossing and handling of larvae

For each experimental cross, approximately 50 virgin females and 15–25 males of the desired genotypes were confined into a bottle containing standard potato diet with yeast. Crosses were transferred into new bottles every second day and kept at 25 °C with 40–70% relative humidity. Overexpression of genes in larval offspring was enhanced using the *GAL4/UAS* system. Immediately after egg deposition (AED), bottles were incubated at 29 °C. After 4–6 days, larvae were collected from bottles and placed into water-containing Petri dishes where they were staged under a stereomicroscope (Andres and Thummel, 1994) and placed on ice for experimental procedure. To prepare for *in vivo* microscopy or bleeding and to ensure release of sessile hemocytes (Makhijani et al., 2011), selected larvae were gently washed using a paintbrush, first in 70% ethanol and then in ice cold tap water.

2.4. Hanging drop and clot preparation

Clot preparations were prepared as described previously (Bidla et al., 2007) using a hanging drop method on glass slides. Timing of clot formation is according to the time under which the hemolymph was forming in the hanging drop; '0 min' demarks the time at which hemolymph clotted for 30 sec then was immediately collected for imaging after the glass slide had been overturned while the '5 min' time point demarks the hemolymph was hanging for 5 min before collection, etc. After the glass slide had been reversed, hanging drops were immediately imaged under standardized illumination conditions using a stereomicroscope to look at clotting macroscopically. Alternatively, an 18 × 18 mm cover slip was used to gently collect the clot from the surface of the hemolymph droplet and transferred to a new glass slide containing 30 µl of stains such as PNA, Hoechst or Phalloidin and observed microscopically.

2.5. Bleeding of larvae

To collect blood cells, 3–5 third instar larvae per genotype were placed together in the wells of a 12-well glass slide, containing 5 µl of ice-cold Ringer's solution and bled as described above. Eight µl of the blood-ringer suspension were transferred onto new multiwell glass slides and incubated in a humidity chamber at room temperature. The time blood cells were allowed to attach depended on the type of cell that was being analyzed: 2–5min for CCs and 10 min for plasmatocytes. After their incubation, samples were either sealed by a cover glass for immediate microscopy or fixed for immunohistochemistry.

2.6. Immunohistochemistry

The protocol used for hemocyte immunostaining is described in detail in (Lesch et al., 2007) however, in order to better visualize CCs, we optimized the fixation protocol by first adding 10 µl of PBS and subsequently 10 µl of ice-cold methanol. This extra step reduced the partial dissolution of crystals which usually occurred after cells were treated with 0.1% Triton X-100 (Sigma-Aldrich). To image plasmatocytes, we used P1/Nimrod C1 (Kurucz et al., 2007) antibodies kindly

provided by István Andó. The *PPO2-GFP* construct created for this study was validated with the C1 (HC12F6) antibody (Willott et al., 1994) from Tina Trenczek. When necessary, we amplified the signals from Tg-GFP, PPO2-GFP and Glt-GFP in fixed hemocytes by using either of two GFP-specific polyclonal antibodies (Alexa Fluor 488, Invitrogen, or A11122, Invitrogen (1:500)). Primary antibodies were visualized with Cy2-conjugated goat anti-mouse polyclonal antibody (1:600, Millipore) or Alexa Fluor 647 donkey anti-rabbit polyclonal antibody (1:500, A31573, Invitrogen) diluted in PBS containing 3% bovine serum albumin (ThermoFischer Scientific). To visualize clots, TRITC-labeled peanut agglutinin (PNA from Sigma, 1:50) or CY5-labeled PNA (Bio-Nordika, 1:50) was mixed with Hoechst 33258 (Sigma-Aldrich, 1:1000) and Ringer's solution. After 10 min in the hanging drop, the clot was captured on a coverslip and was immersed into 3 µl of propidium iodide (0,01 mg ml-1, Sigma P-4170) containing *Drosophila* Ringer's and placed on a microscope slide.

2.7. Microscopy and image analysis

Hanging drops were imaged with a DFC 300Fx digital camera using Firecam imaging software (version 3.4.1) through a MZ16 stereomicroscope (Leica) set to 1.6x magnification. Propidium iodide stained cells were imaged through an Axioscope UV microscope (Zeiss). Live hemocytes and clots were imaged using an Axioplan2 light and UV microscope (Carl Zeiss) set to phase contrast with a 63x oil immersion objective and a Hamamatsu ORCA digital camera controlled by Axio Vision Rel.4.8 software. Movies of live crystal cells were recorded by AxioCam MRc camera adapted to an inverted fluorescence microscope (Zeiss) equipped with a 63x 1.4 DIC oil immersion objective. The system was controlled by the software SlideBook6 for acquisition and image processing. Confocal imaging was conducted through a Plan-Apo 63x/1.40 Oil DIC objective attached to an inverted LSM 800 Airyscan microscope (Zeiss), which was controlled by the ZEN blue 2.1 software. The latter software was also used to select and enhance particular slices and create maximum intensity projections of Z-stacks.

2.8. Image processing and statistical analysis

When needed, both still images and movies of blood cells were enhanced using ImageJ version 1.8.0_172. Vesicle sizes were assessed using the straight line tool in ImageJ (Morrow et al., 2008). Fifty vesicles were measured per protein using the line tool in ImageJ and the results were recorded and processed in GraphPad Prism. Cell profiler 3.0 was used to determine the correlation coefficients of relative intensity colocalization which determined signal overall of the green and red channels using the Rank-Weight Coefficient (Lamprecht et al., 2007). Statistical analysis and graphs were assessed and produced using GraphPad Prism software, version 8.0. Z-stacks of selected images were exported to Imaris v. 9.2 software (Bitplane AG, Zurich, Switzerland) and made into 3D movies. All experiments were performed a minimum of three times with the majority of experiments having been performed more frequently.

3. Results

3.1. Clot formation and melanization are independent

As previously published by our lab (Bidla et al., 2009), drops of hemolymph collected from wild type (w^{1118}) *Drosophila* larvae gradually darken (Fig. 1A) leading to melanized small spots and clot strands (arrows in Fig. 1B). In blood samples from animals heterozygote for $PPO1^{Bc}$ however, hemolymph and clot strands did not melanize. This is due to the fact that *Bc* is a gain-of-function allele of PPO1 driving crystal cells to spontaneous melanization thereby depleting the animal's PO reservoir (Dudzic et al., 2015; Neyen et al., 2015). Microscopically, in wild type samples, melanized blood cells and fragments could be

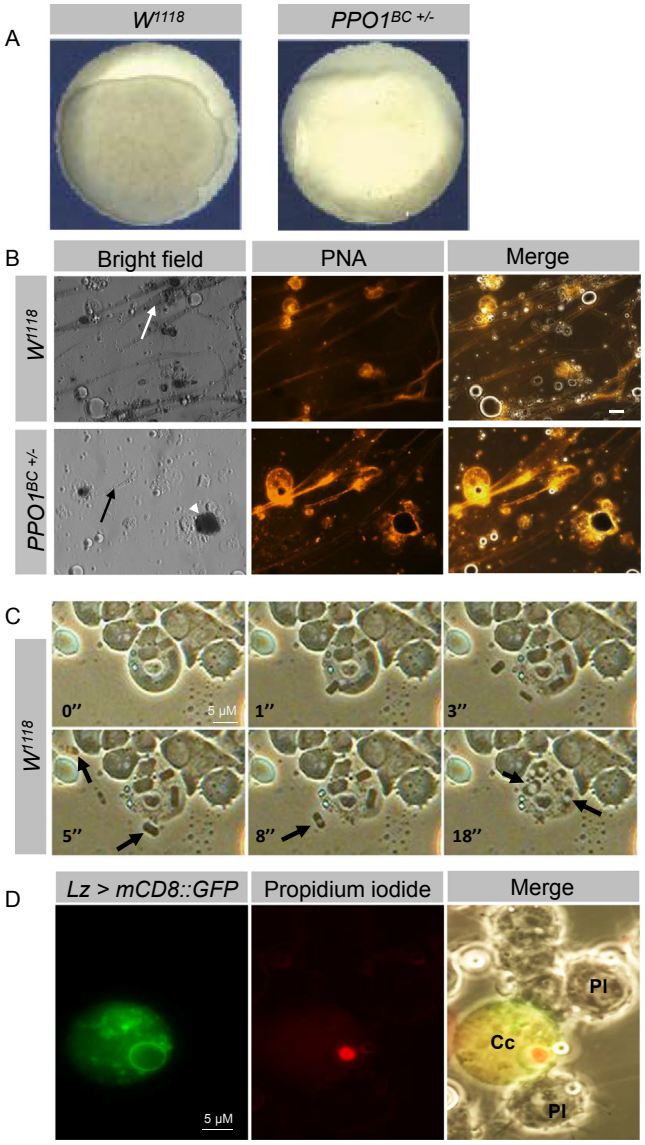

Fig. 1. Formation of *Drosophila* clots involves formation of the clot matrix and melanization. (A) Hemolymph clots were visualized macroscopically on multiwell slides (4 mm diameter) and microscopically (B, clot fibers are indicated by arrows). Melanization, visible in the bright field, was restricted to a subset of the clot, visualized with PNA, and was absent in hemolymph from a mutant that lacks crystal cells (Black cells; $PPO1^{BC\ +/-}$, note that precociously activated crystal cells were still visible as melanized spots in B, arrowhead). (C) Rupture of CCs, release and dissolution of crystals could be followed in real time (crystals are indicated by arrows, see also movie S1, which was recorded 5 min post bleeding, the duration of the movie is 18, sec, the time for the stills is indicated in sec). (D) After release and dissolution of the crystals, empty CCs retained mCD8-GFP on their surface and contained intact, condensed nuclei demonstrated through propdium iodide staining (Pl: Plasmatocytes, CC: crystal cell, scale bar 10 µm in B and 5 µm in C-D). The data show representative images; similar findings were replicated in at least 3 independent experiments.

seen both outside and within the clot fibers confirming earlier observation ((Neyen et al., 2015; Scherfer et al., 2004), Fig. 1B upper row). In contrast, melanization of clots captured from $PPO1^{Bc}$ hemolymph was limited to bigger round structures, most likely single CCs, which were phagocytosed by plasmatocytes ((Neyen et al., 2015; Scherfer et al., 2004); Fig. 1B lower row, fibers and activated CCs indicated by arrow and arrowhead, respectively). Fibers were also visualized using fluorescently-labeled peanut agglutinin (PNA), which detected clots in both $PPO1^{Bc}$ and wild type preparations. Melanization

occurred through the release of PPO-containing crystals after CC rupture, confirming earlier observations (Bidla et al., 2007), which subsequently led to crystal dissolution and melanization of the wound site (real time microscopy stills in Fig. 1C and movie S1). CC rupture usually occurred within the first 5 min after bleeding however, not all CCs were fated to rupture in response to clot formation most likely due to differences in ROS-dependent JNK-signaling (Bidla et al., 2007; Myers et al., 2018). Notably, during dissolution, the central core of the crystal appeared to dissolve faster than the flanking regions, which in some cases led to the crystal breaking apart from the mid-region (arrows in Fig. 1C and movie S2). While some mammalian innate immune cells such as neutrophils and eosinophils release nuclear or mitochondrial DNA (Goldmann and Medina, 2012), CCs retained their nuclear DNA, in line with our previous observations that DNA from CCs does not contribute to *Drosophila* clots ((Bidla et al., 2005), Fig. 1D). Although crystals and most of the cytosolic content were lost after CC rupture, expression of membrane-bound GFP showed that some remnants of membrane structures, including the nuclear membrane and the surface membrane, remained detectable (Fig. 1D).

Supplementary data related to this article can be found at https://doi.org/10.1016/j.ibmb.2019.04.007.

3.2. GFP-tagged lines of clotting factors

We established *Drosophila* lines that contain GFP-tagged versions of three proteins under control of the yeast Gal4/Upstream Activating Sequence (UAS) system—Transglutaminase-A (*UAS-Tg::GFP*; *UAS- Tg-GFP*), Glutactin (*UAS-Glt::GFP*; *UAS-Glt-GFP*) and PPO2 (*UAS-PPO2::GFP*; *UAS-PPO2-GFP*)—in order to follow their role when secreted as clotting factors (Supplemental Fig. 1). To analyze expression in hemocytes, we expressed *Tg-GFP* and *Glt-GFP* in plasmatocytes using the Hemolectin driver (*HmlΔGAl4*) and *PPO2-GFP* in CCs using the Lozenge driver (*LzGal4*).

3.3. Non-conventional release of Tg from hemocytes

When expressed in plasmatocytes (*HmlΔGAl4 > UAS-Tg::GFP*), Tg showed a cytoplasmic, as well as a ring-like pattern both in light and confocal microscopy (Fig. 2). During an early stage of clot formation, ring-like expression was found inside hemocytes (arrows in Fig. 2A and C, arrows), including in some cellular extensions (arrows, Fig. 2B) of some but not all cells. The ring-like pattern is in line with previous findings in which association of Tg-A to vesicles was shown to be mediated by N-myristoylation and subsequent S-palmitoylation, which allows binding to multi-vesicular body-like structures on their cytosolic site (Shibata et al., 2017). Enriched expression in parts of the filopodia (arrow in Fig. 2B) may indicate formation of microparticles, which are released from hemocytes during coagulation of the hemolymph (Theopold and Schmidt, 1997). Confocal microscopy revealed that there were many large vesicles in the cell that eventually budded off (arrows and asterisks, Fig. 2C). Additionally, the cells' surface labeled positive for Tg-GFP when non-permeabilized cells were fixed and labeled for surface-GFP (Fig. 4D) indicating that at least some Tg remained cell-bound after release (compare also Supplemental Fig. 2).

3.4. Transglutaminase-A and Glutactin use distinct modes of externalization

In mammalian cells, tissue transglutaminase (tTG) is exported via recycling endosomes (Zemskov et al., 2011). We found that upon expression in plasmatocytes, a sub-fraction of *Drosophila* Tg-A-containing vesicles displayed endosomal characteristics as determined by close association with mCherry::2xFYVE (FYVE, (Jean et al., 2012)) — a marker for vesicles that contain PI(3)P which is enriched in recycling endosomes (Fig. 3A). While Tg expression led to ring-like patterns with partial colocalization to the FYVE marker, classically secreted Glt-GFP

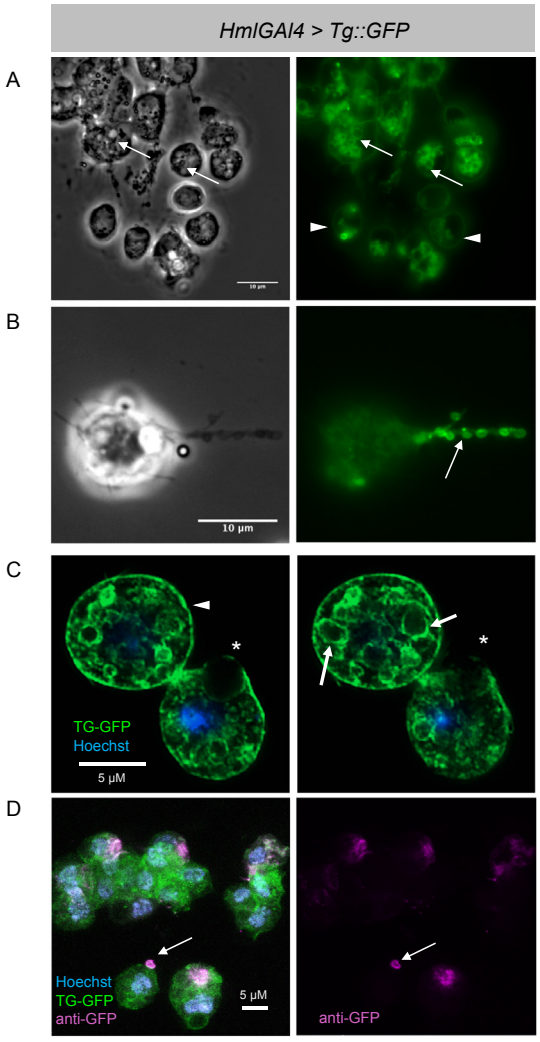

Fig. 2. Hemocyte transglutaminase is associated with vesicles and the cell surface. (A–B) Hemocyte-specific expression of Tg (*HmlΔGAl4 > UAS-Tg::GFP*) showed a vesicular, ring-like expression in live cells and migration of Tg-containing vesicles to cellular protrusions (arrows in A-B) at early stages (5 min after bleeding) as well as signals at the cell periphery (arrowheads in A). (C) Confocal microscopy confirmed the ring-like expression of Tg signals (arrows) and an early stage of vesicle release (asterisks in D, cells fixed with methanol/acetone, two consecutive layers are shown). Potential cell surface signals are indicated by arrowheads (scale bar 10 µm in A-C and 5 µm in D). (D) Non-permeablized cells fixed and stained with anti-gfp and a secondary antibody coupled to Cy5. Cells were imaged using Confocal microscopy and demonstrate that Tg-GFP is seen outside of the cell and bound to the cell surface. A ring-like structure was captured being secreted as indicated by the arrow. The data show representative images; similar findings were replicated in at least 3 independent experiments.

localized to smaller vesicles mostly independent of FYVE (Fig. 3 A and C). Moreover, the Glt-GFP signal filled the complete vesicle indicating luminal localization in hemocytes which supports the classical secretion of Glt (see arrow in Fig. 3A). Localization of Tg-GFP to FYVE + vesicles was further confirmed using confocal imaging which revealed the presence of vesicular fusions that are characteristic for a compound mode of secretion (Fig. 3B and (Pickett and Edwardson, 2006)). In addition, colocalization was greater in cells containing Tg-GFP and the mCherry::FYVE marker than those which contained Glt-GFP instead (Fig. 3C). Furthermore statistical analysis revealed median vesicle diameters in Glt-GFP and Tg-GFP were 3.68 and 7.96 pixels respectively; the two groups differed significantly (Mann–Whitney $U = 47$, $n1 = n2 = 31$, $P < 0.0001$ two-tailed) (Fig. 3D). These results

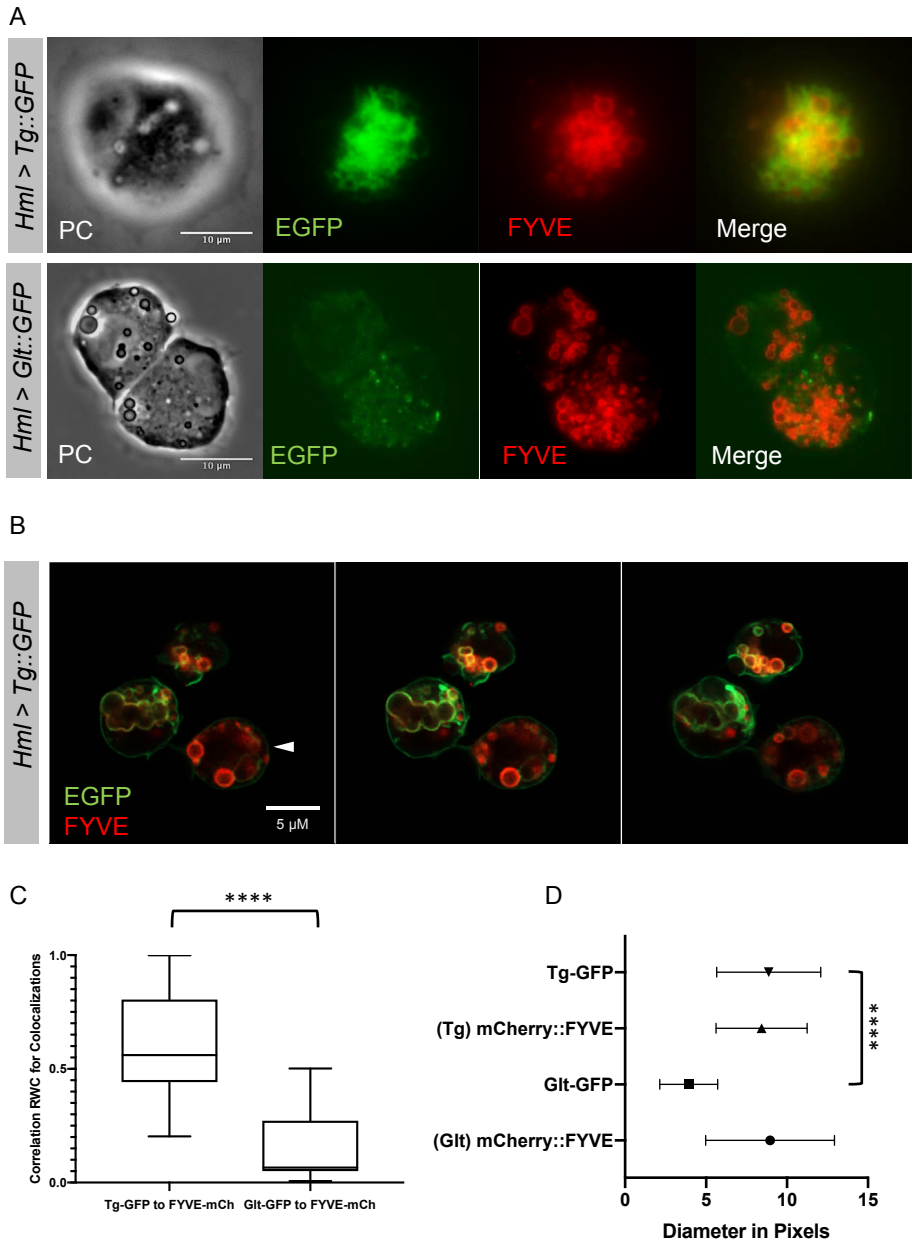

Fig. 3. Tg shows partial colocalization with a marker for nonclassical secretion. (A) Upon expression of *HmlΔGAl4 > UAS-Tg::GFP,* mCherry::2xFYVE (A, upper part, fluorescence microscopy of live cells) or *HmlΔGAl4 > UAS-Glt::GFP,* mCherry::2xFYVE (A, lower part) using a hemocyte specific driver, Tg, but not Glt, colocalized with a marker, FYVE (*mCherry::2xFYVE*), which binds PI(3)P on vesicles destined for non-classical secretion. (B) Three consecutive confocal stacks *HmlΔGAl4 > UAS-Tg::GFP,* mCherry::FYVE. The cell surface signal is indicated by an arrowhead (scale bar 10 μm in A and 5 μm in B). (C) Quantification of the relative intensity of overlapping signals between the green and red channels using Rank-Weight correlation coefficients (RWC). Several images of Tg-GFP (n = 22) or Glt-GFP (n = 13) were assessed to determine their RWC to mCherry::FYVE. The box plot demonstrates that Tg-GFP (0.6096, ± 0.2467) was significantly more likely to colocalize with the FYVE-mCh than was Glt-GFP (0.1591, ± 0.1810, two sample *t*-test, $p < 0.0001$). (D) The average diameter of the vesicles formed for Glt or Tg, as compared to the mCherry::FYVE vesicles showed that Tg vesicles were significantly larger than Glt vesicles (Mann–Whitney U = 47, n1 = n2 = 31, P < 0.0001 two-tailed) and that both had medians of comparablely sized vesicles for mCherry::FYVE. These data show representative images; similar findings were replicated in at least 3 independent experiments.

confirmed that Tg was in significantly larger vesicular, ring-like structures, that Tg and Glt localized to different subcellular compartments and that they were secreted from the hemocyte via non-classical and classical secretion, respectively.

3.5. PPO2-GFP is found in cytosolic crystals

Analysis of PPO2-GFP patterns in CCs revealed substantial variability in expression. In some CCs, localization of PPO2 was mostly in the cytosol (Fig. 4A upper and middle part, and C) while in other cells, crystals of different numbers and sizes had formed (Fig. 4A lower part, D, movie S4), replacing the cytosolic distribution. Crystals were devoid of any mCD8-mRFP signal confirming their membrane-free nature (Rizki et al., 1980). In some crystals, in particular after cell rupture, a central core with either lower or absent levels of PPO2-GFP was visible and congruent with our previous observations which revealed that crystals start dissolving from within (Fig. 4B and D arrows, compare to Fig. 1C, lower row) and were released through cell rupture (suppl. movie S2). In third instar larvae, the number of crystals varied between cells, with most containing 2 or more crystals and some containing up to 10 (or more) crystals (Fig. 4E).

Supplementary data related to this article can be found at https://doi.org/10.1016/j.ibmb.2019.04.007.

3.6. Crystals mature during ontogeny

One possible explanation for the variable morphology of PPO2 expression is that cytosolic expression corresponds to early stages of CC development and the appearance of crystals takes time to develop and is therefore characteristic of later developmental stages. In line with this hypothesis, we detected cytosolic PPO2 expression at early stages of CC development through the integuments of live larvae (Fig. 5A and 24 h after egg deposition: AED), which was replaced by the characteristic crystalline patterns of later stages (Fig. 5A, 48–96 h larvae AED). This was further confirmed when we compared the relative abundance of crystal-containing CCs in bled larvae increasing over developmental time (Fig. 5B for statistical analysis and C, which shows the scoring scheme; note, 24 h larvae were too small to bleed).

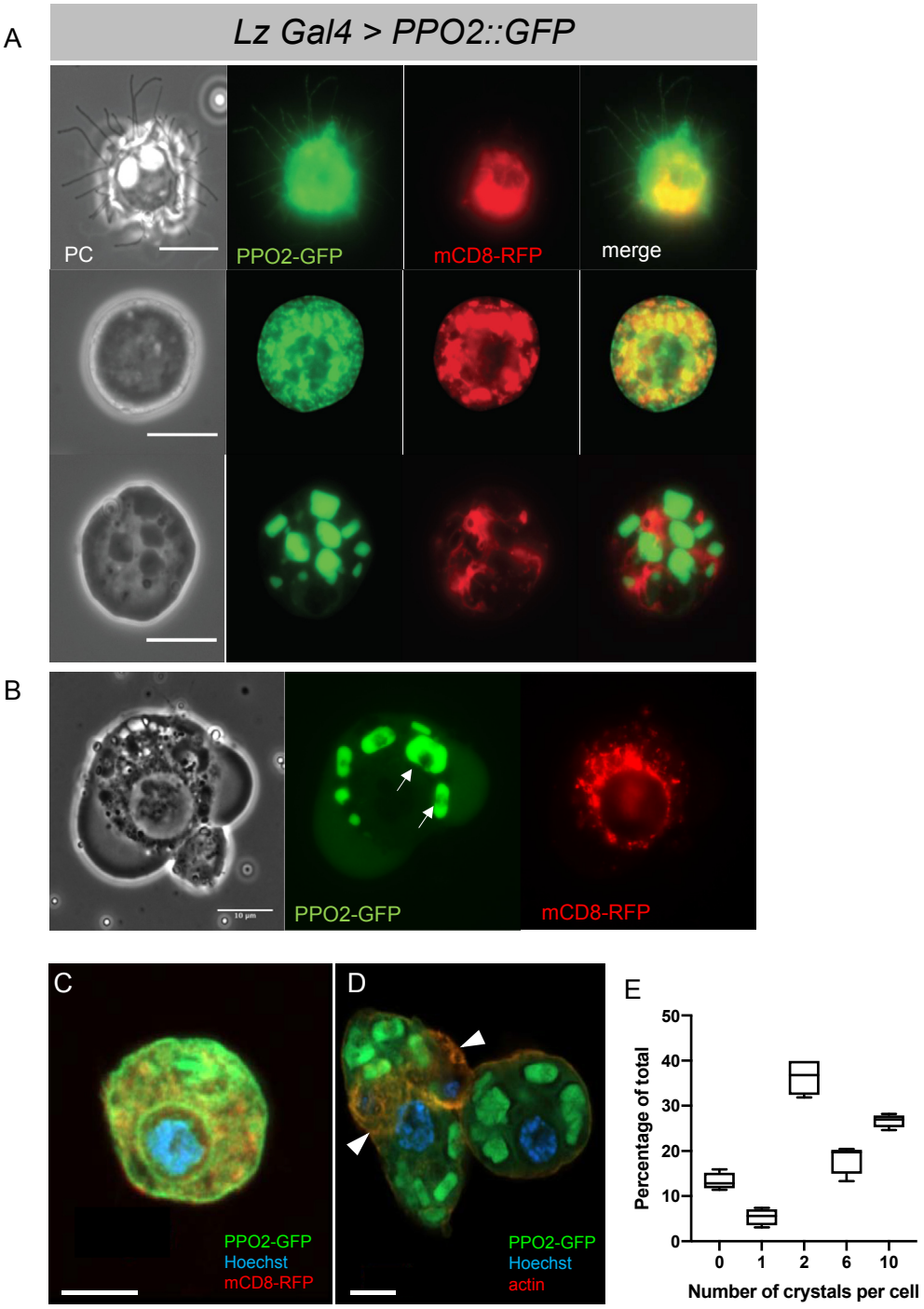

Fig. 4. Upon expression in CCs, PPO2-GFP is incorporated into crystals. (A–D) *mCD8-RFP* and *PPO2-GFP* (*Lz GAl4 > UAS-PPO2::GFP*) were expressed in CCs using *Lz-Gal4* and their expression patterns were analyzed in live cells using epifluorescence microscopy. PPO2-GFP showed different patterns ranging from almost completely cytosolic (Fig. 4A, upper part and C), partially cytosolic (Fig. 4a, middle) or strong labelling of well-defined crystals (Fig. 4A, lower part and D). In addition, cell protrusions were seen in Fig. 4A upper part and a ruptured cell is seen in Fig. 4B. After rupture, the crystals dissolved reproducing the dimorphic pattern we had observed previously, with a weaker PPO2-GFP signal in the core surrounded by brighter areas (arrows in Fig. 4B compared to Fig. 1C). C–D: Confocal images of CCs expressing *PPO2-GFP* and (C) *mCD8.RFP* or (D) counterstained with phallodin (actin) and Hoechst in (C-D, scale bar 10 µm in A-B and 5 µm in C-E). Two plasmatocytes are seen to be adhereing to the partially activated CC (arrowheads in 4D). (E) Counts of the percentage of CCs found to contain different numbers of crystals in L3 larvae. These data show representative images; similar findings were replicated in at least 3 independent experiments.

3.7. Secretion of clotting factors after bleeding

In order to follow our three proteins of interest during clot formation, we used the GFP-tagged versions of Tg, Glt and PPO2 to follow their release from hemocytes and eventually, into the clot fibers. Importantly by restricting expression of the tagged constructs to hemocytes, we focused their contribution to the clot and did not analyse other non-hemocyte sources. We analyzed samples at 0 and 5 min post incubation in the hanging drop as part of the early clot formation and subsequent time points were deemed to be late clot formation. By time point 5 min, hemocyte-derived Tg had either been incorporated into the clot or had remained bound to the membrane surface of the hemocytes, Glt-GFP was found to be a part of the clot. Their distribution in clots appeared to differ: while Glt showed a homogenous distribution along clot fibers, Tg localized to dot-like structures, similar to what we had previously observed on single cells (Fig. 2 B and D). At 35 min, hemocyte-derived Tg appeared to still remain membrane bound (compare 5′ and 35′ in Fig. 6B), while phenoloxidase had led to melanin production and darkening of the clot (Fig. 6B, phase contrast at 35'), PPO2 had generally started to be released from CCs 5 min after bleeding but was not incorporated into the clot until 15 min post hanging drop (Fig. 6). PPO2-GFP was eventually quenched by the proteolytic activation of PPO and subsequent melanization ((Dudzic et al., 2015; Neyen et al., 2015) and data not shown). Furthermore, while the majority of CCs had ruptured in later time points, empty shells could still be seen to contain dissolving crystals (Figs. 1C and 4A, right part). Since we had previously observed Tg activity in the clot matrix (Lindgren et al., 2008; Wang et al., 2010) we attribute this more widespread

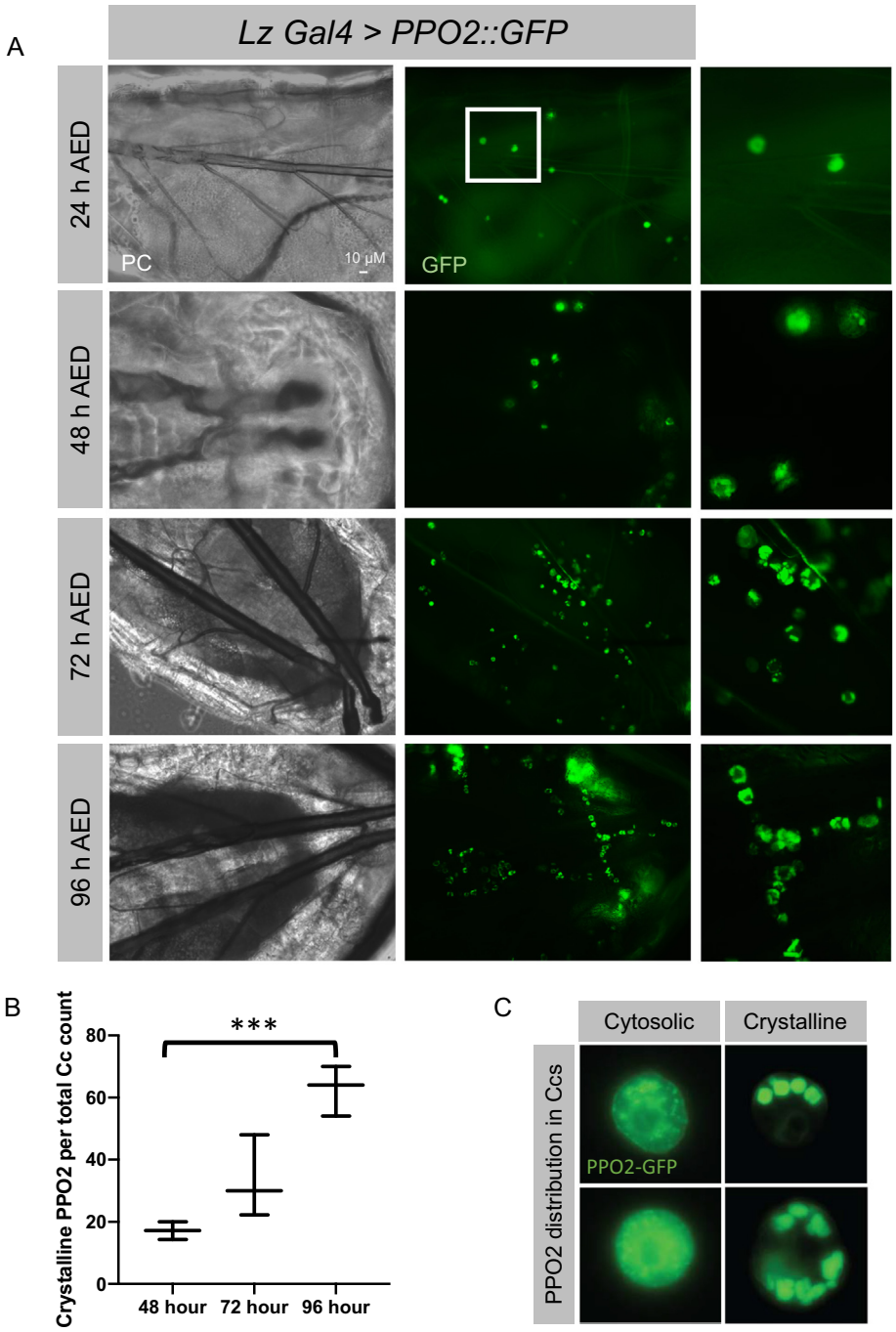

Fig. 5. Redistribution of PPO2-GFP in crystal cells during ontogeny. (A) *Lz Gal4 > UAS-PPO2::GFP* expressing larvae were analyzed at different time points after egg deposition (AED) through the integument of live larvae at 24, 48, 72 and 96 h AED using epifluorescence microscopy and phase contrast (PC). Crystals within CCs increase in frequency from 24 to 96 h during larval development (scale bars 10 µm). The boxed areas are enlarged in the right hand column. (B) The proportion of crystals cells containing cytosolic or crystalline structures quantified at 48, 72 and 96 h from bled larvae. Larvae at 96 h (62.67% ± 8.083, n = 3) had significantly more (45.52%) cells containing crystalline structures over cytosolic PPO2 than 48 h larvae (17.14% ± 2.857, n = 3, twosample *t*-test, $p < 0.001$). (C) A depiction of how crystal cells were scored based on their PPO2 expression pattern for the graph produced in B. The left hand panel was scored as cytosolic while the right-hand panel was scored as crystalline. The data show representative images; similar findings were replicated in at least 3 independent experiments.

activity to other non-hemocyte sources. Hemocyte-derived Tg may in fact play a role similar to its homologue in horseshoe crabs, where it serves to crosslink two cell surface proteins from hemocytes (proxins 1 and 2) to the matrix component (coagulin, (Osaki et al., 2002)). Glt was likely a part of the early clot while PPO2 acted at later time points to harden clot fibers ultimately leading to melanization.

4. Discussion

In this study, we created tagged versions for three secreted proteins, all of which have been previously found to contribute to formation of hemolymph clots. The classically released Glutactin was secreted early on during clot formation from small cellular vesicles and appeared to be a part of clot fibers, similar to Fondue and Idgf3 (Bajzek et al., 2012; Kucerova et al., 2016; Lindgren et al., 2008). However, our major focus in this work was on two proteins which lack a signal peptide yet are both essential contributors to clot formation. Similar to its mammalian functional equivalent factor XIIIa, *Drosophila* transglutaminase cross-links the clot matrix and aids in preventing bacterial dissemination from wounds (sepsis, (Lindgren et al., 2008; Loof et al., 2011a; Loof et al., 2011b; Wang et al., 2010)). Although less is known about the subcellular distribution of factor XIIIa, *Drosophila* Tg-A shares similarities with mammalian tissue transglutaminase: (1) it localized to vesicles that are rich in PI(3)P and may therefore also be picked up by recycling endosomes on the way to the cell surface (Fig. 2 and (Zemskov et al., 2011)) and (2) *Drosophila* transglutaminase remains – at least in part – when released from hemocytes– membrane bound (Figs. 2 and 3 and (Shibata et al., 2017)). There are however molecular differences between *Drosophila* Tg and human tTg, for example in the mode of binding Tg to the cytosolic site of endosomes mediated via lipid modification in

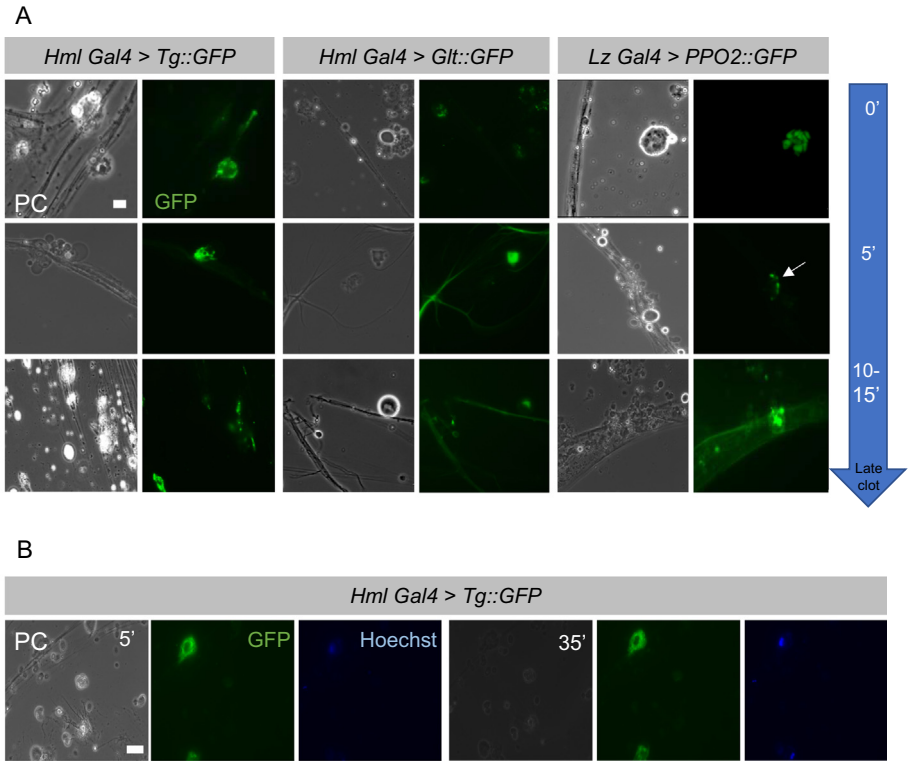

Fig. 6. Secretion of clotting factors during clot formation. (A) GFP-tagged versions of clotting factors were traced at the indicated time points post-bleeding using phase contrast (PC) and epi-fluorescence microscopy of live cells (GFP). Clots were prepared and collected at 0 min, 5 min and 10–15 min. Tg can be seen being incorporated in clot fibers at 0 min and 10–15min. Glt was incorporated into the clot at 5 min and remained there during later time points. PPO2 is seen in an intact CC at 0 min next to clot fibers, a CC has ruptured and activated crystals are seen stuck in the clot at 5 min (see arrow) and PPO2 is released and incorporated into the clot after 10–15 min in the hanging drop (scale bar 10 μm). (B) Being that Tg was not always seen to be released beyond the cell surface of the hemocyte, we checked a hanging drop at both 5 min (left) and 35 min (right). During this time, Tg remained membrane bound despite being attached to the clot fibers. Due to the melanization process and the same exposure time, the Phase Contrast (PC) has darkened substantially at timepoint 35 min. The data show representative images; similar findings were replicated in at least 3 independent experiments.

flies (Shibata et al., 2017) and a dedicated lipid-binding domain in tTG (Zemskov et al., 2011). In addition, *Drosophila* Tg has been found to be released via exosomes (Shibata et al., 2017), and larger vesicles, which we observe here (Figs. 2 and 6). This kind of secretion may serve the same function as platelet microparticles during blood clotting (Theopold and Schmidt, 1997). Further use of GFP-tagged transglutaminase will allow us to determine its contribution to clot formation from other tissues. The second protein without a signal peptide, PPO2 has previously been shown to be released by rupture of crystal cells (Bidla et al., 2007), which we documented in real time. Of note, we found PPO2 to be unevenly distributed within crystals indicating that the crystals are not homogenous and may contain components other than PPO2. Taken together, our characterization of the subcellular distribution of Tg and PPO2 provides a first glimpse of the variability of modes of protein secretion from hemocytes in an immune scenario.

We anticipate that our work will provide insights into the variable use of classical and non-classical secretion and its evolutionary dynamics in the role of clot formation during wound healing. The results presented in our clotting assay allow us to outline the sequence of events during the first 10–15 min of clot formation, which is unprecedented in insects. One caveat, is the fact that clotting involves covalent crosslinking activities including PO and Tg, which have the potential to structurally interfere with GFP fluorescence. In addition, melanin quenches the GFP signal. Therefore, later stages of clotting may not be covered by our visual approach. In addition, while our choice of drivers was guided by what is known about expression of the respective proteins, using CRISPR/Cas engineered gene traps will reflect endogenous expression more closely, although possibly at the expense of signal strength. Expression via UAS on the other hand, allows expression in additional secretory tissues and therefore, testing the general implication of our findings both *in vivo* and in cell culture.

Insect hemocytes are usually described as “macrophage-like cells” and consequently, the major focus has been on their phagocytic capacity. One major goal of our work was to establish hemocytes as equally important secretory cells, akin to granulocytes in mammals (Acharya and Ackerman, 2014). Mammalian innate immune cells are amongst the rare cell types that harbor crystalline inclusions. Most relevant for immunity, eosinophils contain crystals composed of major basic protein 1 (MBP1), a cytotoxic protein and one of the major constituents of eosinophils (Soragni et al., 2015). Upon release, MBP1 initially dissolves followed by the formation of amyloid-like deposits on microbial surfaces, which kills them. Control of MBP1's cytotoxic activity is via incorporation into larger extracellular aggregates in which MBP1 is inactive. There are functional similarities between granulocytes and hemocytes as well as between MBP1 and *Drosophila* PPO2, namely their (1) intracellular storage in crystalline form, (2) the cytotoxic activity and ultimately, (3) their incorporation into extracellular aggregates. In contrast to PPO2 crystals, MBP1 crystals are surrounded by a membrane (Soragni et al., 2015). A second type of crystals in eosinophils Charcot Leyden crystal, which also lack a membrane, form during cell rupture (Ueki et al., 2018). Although Charcot Leyden crystals have been known for over 150 years and their major constituent is known, galectin 10, their function remains somewhat elusive (Ueki et al., 2018).

Altogether, we provide new tools which we used to study secretion in an innate immune context and expect that these tools will expand our knowledge of the development and regulation of secretory processes in insect as well as mammalian immune cells.

Funding

This work was supported by the Swedish Research Council (VR-2010-5988 and VR 2016-04077) and the Swedish Cancer Foundation (CAN 2010/553 and CAN 2013/546).

Acknowledgments

We would like to thank Arne Jodlauk, Eike Heydorn and Anna Woitalla and Dianxiang Li for help with this project, Stina Höglund and the Imaging facility at Stockholm University for support with all aspects of microscopy and Einar Ólafsson for his help with Cell Profiler. We would also like to thank Dilan Khalili and Roger Karlsson for their critical thoughts and feedback during the experimental process.

Appendix A. Supplementary data

Supplementary data to this article can be found online at https://doi.org/10.1016/j.ibmb.2019.04.007.

References

Acharya, K.R., Ackerman, S.J., 2014. Eosinophil granule proteins: form and function. J. Biol. Chem. 289, 17406–17415.

Anderl, I., Vesala, L., Ihalainen, T.O., Vanha-Aho, L.M., Ando, I., Ramet, M., Hultmark, D., 2016. Transdifferentiation and proliferation in two distinct hemocyte lineages in *Drosophila melanogaster* larvae after wasp infection. PLoS Pathog. 12, e1005746.

Andres, A.J., Thummel, C.S., 1994. Methods for quantitative analysis of transcription in larvae and prepupae. Methods Cell Biol. 44, 565–573.

Arefin, B., Kucerova, L., Dobes, P., Markus, R., Strnad, H., Wang, Z., Hyrsl, P., Zurovec, M., Theopold, U., 2014. Genome-wide transcriptional analysis of *Drosophila* larvae infected by entomopathogenic nematodes shows involvement of complement, recognition and extracellular matrix proteins. J. Innate Immun. 6, 192–204.

Arefin, B., Kucerova, L., Krautz, R., Kranenburg, H., Parvin, F., Theopold, U., 2015. Apoptosis in hemocytes induces a shift in effector mechanisms in the *Drosophila* immune system and leads to a pro-inflammatory state. PLoS One 10, e0136593.

Bajzek, C., Rice, A.M., Andreazza, S., Dushay, M.S., 2012. Coagulation and survival in *Drosophila melanogaster* fondue mutants. J. Insect Physiol. 58, 1376–1381.

Bidla, G., Dushay, M.S., Theopold, U., 2007. Crystal cell rupture after injury in *Drosophila* requires the JNK pathway, small GTPases and the TNF homolog Eiger. J. Cell Sci. 120, 1209–1215.

Bidla, G., Hauling, T., Dushay, M.S., Theopold, U., 2009. Activation of insect phenoloxidase after injury: endogenous versus foreign elicitors. J. Innate Immun. 1 310-308.

Bidla, G., Lindgren, M., Theopold, U., Dushay, M.S., 2005. Hemolymph coagulation and phenoloxidase in *Drosophila* larvae. Dev. Comp. Immunol. 29, 669–679.

Brand, A.H., Perrimon, N., 1993. Targeted gene expression as a means of altering cell fates and generating dominant phenotypes. Development 118, 401–415.

Crozatier, M., Vincent, A., 2011. *Drosophila*: a model for studying genetic and molecular aspects of haematopoiesis and associated leukaemias. Dis. Model. Mech. 4, 439–445.

Dudzic, J.P., Kondo, S., Ueda, R., Bergman, C.M., Lemaitre, B., 2015. *Drosophila* innate immunity: regional and functional specialization of prophenoloxidases. BMC Biol. 13, 81.

Elrod-Erickson, M., Mishra, S., Schneider, D., 2000. Interactions between the cellular and humoral immune responses in *Drosophila*. Curr. Biol. 10, 781–784.

Goldmann, O., Medina, E., 2012. The expanding world of extracellular traps: not only neutrophils but much more. Front. Immunol. 3, 420.

Honti, V., Csordas, G., Kurucz, E., Markus, R., Ando, I., 2014. The cell-mediated immunity of *Drosophila melanogaster*: hemocyte lineages, immune compartments, microanatomy and regulation. Dev. Comp. Immunol. 42, 47–56.

Jean, S., Cox, S., Schmidt, E.J., Robinson, F.L., Kiger, A., 2012. Sbf/MTMR13 coordinates PI(3)P and Rab21 regulation in endocytic control of cellular remodeling. Mol. Biol. Cell 23, 2723–2740.

Korayem, A.M., Fabbri, M., Takahashi, K., Scherfer, C., Lindgren, M., Schmidt, O., Ueda, R., Dushay, M.S., Theopold, U., 2004. A *Drosophila* salivary gland mucin is also expressed in immune tissues: evidence for a function in coagulation and the entrapment of bacteria. Insect Biochem. Mol. Biol. 34, 1297–1304.

Krautz, R., Arefin, B., Theopold, U., 2014. Damage signals in the insect immune response. Front. Plant Sci. 5, 342.

Kucerova, L., Broz, V., Arefin, B., Maaroufi, H.O., Hurychova, J., Strnad, H., Zurovec, M., Theopold, U., 2016. The *Drosophila* chitinase-like protein IDGF3 is involved in protection against nematodes and in wound healing. J. Innate Immun. 8 (2), 199–210.

Kurucz, E., Markus, R., Zsamboki, J., Folkl-Medzihradszky, K., Darula, Z., Vilmos, P., Udvardy, A., Krausz, I., Lukacsovich, T., Gateff, E., Zettervall, C.J., Hultmark, D., Ando, I., 2007. Nimrod, a putative phagocytosis receptor with EGF repeats in *Drosophila* plasmatocytes. Curr. Biol. 17, 649–654.

Lamprecht, M.R., Sabatini, D.M., Carpenter, A.E., 2007. CellProfiler: free, versatile software for automated biological image analysis. Biotechniques 42, 71–75.

Lesch, C., Goto, A., Lindgren, M., Bidla, G., Dushay, M.S., Theopold, U., 2007. A role for Hemolectin in coagulation and immunity in *Drosophila melanogaster*. Dev. Comp. Immunol. 31, 1255–1263.

Lindgren, M., Riazi, R., Lesch, C., Wilhelmsson, C., Theopold, U., Dushay, M.S., 2008. Fondue and transglutaminase in the *Drosophila* larval clot. J. Insect Physiol. 54, 586–592.

Loof, T.G., Morgelin, M., Johansson, L., Oehmcke, S., Olin, A.I., Dickneite, G., Norrby-Teglund, A., Theopold, U., Herwald, H., 2011a. Coagulation, an ancestral serine protease cascade, exerts a novel function in early immune defense. Blood 118, 2589–2598.

Loof, T.G., Schmidt, O., Herwald, H., Theopold, U., 2011b. Coagulation systems of invertebrates and vertebrates and their roles in innate immunity: the same side of two coins? J. Innate Immun. 3, 34–40.

Makhijani, K., Alexander, B., Tanaka, T., Rulifson, E., Bruckner, K., 2011. The peripheral nervous system supports blood cell homing and survival in the *Drosophila* larva. Development 138, 5379–5391.

Markus, R., Kurucz, E., Rus, F., Ando, I., 2005. Sterile wounding is a minimal and sufficient trigger for a cellular immune response in *Drosophila melanogaster*. Immunol. Lett. 101, 108–111.

Morrow, E.H., Leijon, A., Meerupati, A., 2008. Hemiclonal analysis reveals significant genetic, environmental and genotype x environment effects on sperm size in *Drosophila melanogaster*. J. Evol. Biol. 21, 1692–1702.

Myers, A.L., Harris, C.M., Choe, K.M., Brennan, C.A., 2018. Inflammatory production of reactive oxygen species by *Drosophila* hemocytes activates cellular immune defenses. Biochem. Biophys. Res. Commun. 505, 726–732.

Neyen, C., Binggeli, O., Roversi, P., Bertin, L., Sleiman, M.B., Lemaitre, B., 2015. The Black cells phenotype is caused by a point mutation in the *Drosophila* pro-phenoloxidase 1 gene that triggers melanization and hematopoietic defects. Dev. Comp. Immunol. 50, 166–174.

Olson, P.F., Fessler, L.I., Nelson, R.E., Sterne, R.E., Campbell, A.G., Fessler, J.H., 1990. Glutactin, a novel *Drosophila* basement membrane-related glycoprotein with sequence similarity to serine esterases. EMBO J. 9, 1219–1227.

Osaki, T., Okino, N., Tokunaga, F., Iwanaga, S., Kawabata, S., 2002. Proline-rich cell surface antigens of horseshoe crab hemocytes are substrates for protein cross-linking with a clotting protein coagulin. J. Biol. Chem. 277, 40084–40090.

Pickett, J.A., Edwardson, J.M., 2006. Compound exocytosis: mechanisms and functional significance. Traffic 7, 109–116.

Rizki, T.M., Rizki, R.M., Grell, E.H., 1980. A mutant affecting the crystal cells in *Drosophila melanogaster*. Wilehm Roux Arch. Dev. Biol. 188, 91–99.

Scherfer, C., Karlsson, C., Loseva, O., Bidla, G., Goto, A., Havemann, J., Dushay, M.S., Theopold, U., 2004. Isolation and characterization of hemolymph clotting factors in *Drosophila melanogaster* by a pullout method. Curr. Biol. 14, 625–629.

Scherfer, C., Qazi, M.R., Takahashi, K., Ueda, R., Dushay, M.S., Theopold, U., Lemaitre, B., 2006. The Toll immune-regulated *Drosophila* protein Fondue is involved in hemolymph clotting and puparium formation. Dev. Biol. 295, 156–163.

Schmid, M.R., Anderl, I., Vo, H.T., Valanne, S., Yang, H., Kronhamn, J., Ramet, M., Rusten, T.E., Hultmark, D., 2016. Genetic screen in *Drosophila* larvae links ird1 function to toll signaling in the fat body and hemocyte motility. PLoS One 11, e0159473.

Shibata, T., Hadano, J., Kawasaki, D., Dong, X., Kawabata, S.I., 2017. *Drosophila* TG-A transglutaminase is secreted via an unconventional Golgi-independent mechanism involving exosomes and two types of fatty acylations. J. Biol. Chem. 292, 10723–10734.

Shibata, T., Kawabata, S.I., 2018. Pluripotency and a secretion mechanism of *Drosophila* transglutaminase. J. Biochem. 163, 165–176.

Soragni, A., Yousefi, S., Stoeckle, C., Soriaga, A.B., Sawaya, M.R., Kozlowski, E., Schmid, I., Radonjic-Hoesli, S., Boutet, S., Williams, G.J., Messerschmidt, M., Seibert, M.M., Cascio, D., Zatsepin, N.A., Burghammer, M., Riekel, C., Colletier, J.P., Riek, R., Eisenberg, D.S., Simon, H.U., 2015. Toxicity of eosinophil MBP is repressed by intracellular crystallization and promoted by extracellular aggregation. Mol. Cell 57, 1011–1021.

Theopold, U., Krautz, R., Dushay, M.S., 2014. The *Drosophila* clotting system and its messages for mammals. Dev. Comp. Immunol. 42, 42–46.

Theopold, U., Li, D., Fabbri, M., Scherfer, C., Schmidt, O., 2002. The coagulation of insect hemolymph. Cell. Mol. Life Sci. 59, 363–372.

Theopold, U., Schmidt, O., 1997. *Helix pomatia* lectin and annexin V, two molecular probes for insect microparticles: possible involvement in hemolymph coagulation. J. Insect Physiol. 43, 667–674.

Theopold, U., Schmidt, O., Söderhäll, K., Dushay, M.S., 2004. Coagulation in arthropods: defence, wound closure and healing. Trends Immunol. 25, 289–294.

Tokusumi, T., Shoue, D.A., Tokusumi, Y., Stoller, J.R., Schulz, R.A., 2009. New hemocyte-specific enhancer-reporter transgenes for the analysis of hematopoiesis in *Drosophila*. Genesis 47, 771–774.

Ueki, S., Tokunaga, T., Melo, R.C.N., Saito, H., Honda, K., Fukuchi, M., Konno, Y., Takeda, M., Yamamoto, Y., Hirokawa, M., Fujieda, S., Spencer, L.A., Weller, P.F., 2018 Nov 15. Charcot-Leyden crystal formation is closely associated with eosinophil extracellular trap cell death. Blood 132 (20), 2183–2187.

Wang, Z., Wilhelmsson, C., Hyrsl, P., Loof, T.G., Dobes, P., Klupp, M., Loseva, O., Morgelin, M., Ikle, J., Cripps, R.M., Herwald, H., Theopold, U., 2010. Pathogen entrapment by transglutaminase-a conserved early innate immune mechanism. PLoS Pathog. 6, e1000763.

Willott, E., Trenczek, T., Thrower, L.W., Kanost, M.R., 1994. Immunochemical identification of insect hemocyte populations: monoclonal antibodies distinguish four major hemocyte types in manduca sexta. Eur. J. Cell Biol. 65, 417–423.

Zemskov, E.A., Mikhailenko, I., Hsia, R.C., Zaritskaya, L., Belkin, A.M., 2011. Unconventional secretion of tissue transglutaminase involves phospholipid-dependent delivery into recycling endosomes. PLoS One 6, e19414.